E-proceedings of the 38th IAHR World Congress
September 1-6, 2019, Panama City, Panama
doi:10.3850/38WC092019-1900

EXPERIMENTS AND NUMERICAL MODELING OF FIELD-SCALE GEYSERS IN STORMSEWER SYSTEMS

ARTURO S. LEON[1] & SUMIT R. ZANJE[2]

[1,2] Department of Civil and Environmental Engineering,
Florida International University, Miami, Florida, USA
arleon@fiu.edu; szanj001@fiu.edu

ABSTRACT

This paper reports a laboratory and numerical study on violent geysers in a vertical pipe. The laboratory geysers produced consists of a few consecutive violent eruptions within a time frame of a few seconds with heights that may exceed 30 m and with characteristics resembling geysers that occur in actual stormsewer systems (e.g., strongest eruption is not the first one but few eruptions later). In general, the present study shows that once the air pocket breaks through the free surface and produces a water spill, the horizontal pipe flow dynamics, in particular the rapidly changing pressure gradient following the first weak eruption, is driving the entire geyser mechanism. This conference paper is based on the following papers Leon 2016, 2018, Leon et al. 2018, and Chegini and Leon 2019.

Keywords: Combined sewer system; experiment; geyser; numerical simulation; stormwater; two-phase flow.

1 INTRODUCTION

Geysers have been studied over three decades in terms of water phase only or air-water interaction (Guo & Song, 1991; Lewis, 2011; Shao, 2013). These studies include laboratory experiments and numerical modeling. Several of these studies focused on the analysis of dynamic flow conditions under which geysers could occur. Hamam and McCorquodale (1982), Vasconcelos (2005), and Lewis (2011) studied the mechanisms through which air is entrapped in horizontal tunnels. Furthermore, a number of laboratory experiments (Vasconcelos, 2005; Lewis, 2011) have been conducted to produce “spring”-like geysers, however none of these experiments produced large geyser heights as observed in actual stormsewer systems. Spring-like eruptions are characterized by a first strong eruption followed by very rapidly decaying eruptions. Additionally, a number of studies have focused on numerical modeling of geysers. Choi et al. (2014) used a compressible solver in Star-CCM+ for studying spring-like geysers. Moreover, Chan et al. (2018) also used a compressible solver to perform a series of 3D simulations based on experimental results in Cong et al. (2017). Most numerical studies simulated geysers that do not resemble the characteristics of geysers produced in actual stormsewer systems. Recently, Chegini and Leon (2019) utilized OpenFOAM (CFD Direct, 2017) for simulating field-scale geysers and with characteristics resembling those produced in actual stormsewer systems.

In general, previous work has speculated that geysers are driven by the buoyant rise of air pockets in a vertical pipe. The present work shows that once the air pocket breaks through the free surface and produces a water spill, the horizontal pipe flow dynamics drives the entire geyser mechanism. The present work has produced violent geysers in a laboratory setting that resemble those observed in actual stormwater and combined sewer systems (e.g., a few consecutive violent eruptions within a time frame of a few seconds with heights that may exceed 30 m). In a similar way to actual geysers in stormsewer systems, the first eruption of the laboratory geysers was not the strongest in terms of intensity (e.g., height). This paper is divided as follows. First, the experimental setup, the experimental procedure and experimental results are presented. Second, the numerical model is briefly presented. Then, considerations for efficient numerical modeling of geysers is briefly described along comparisons between experimental and numerical results. Finally, the key results are summarized in the conclusion.

2 EXPERIMENTAL WORK

2.1 Experimental Setup

The apparatus for the experimental study is shown schematically in Figure 1. The horizontal and vertical pipe consisted of clear PVC schedule 40 with an internal diameter of 152.4 mm. The upstream tank has a total volume of 1.7 m^3 (450 US gallons) and a maximum operating absolute pressure head of 105.5 m (150 psi). It is worth mentioning that the ratio of initial volume of air to initial volume of water in the present experiments ranged

©2019, IAHR. Used with permission / ISSN 2521-7119 (Print) - ISSN 2521-716X (Online) - ISSN 2521-7127 (USB)

from 4.5 to 7.8, which ratios are much larger than previous experimental investigations on geysers. The upstream tank is connected to the horizontal pipe through a 152.4 mm gate valve, which controls the flow from the head tank. Eight experimental configurations were created by varying three parameters. The first parameter was the vertical pipe length (3, 6, 9 and 12 m), which is the same as the initial water depth in the vertical pipe. The second parameter was the initial water volume in the tank, which were 0.7760 m^3 (205 US gallons) and 0.9615 m^3 (254 US gallons). The third parameter was the initial air absolute pressure head in the upstream tank. Every experimental run was repeated fifteen times, which resulted in a total of 120 experiments. The geyser heights are consistent as shown by the relatively small coefficient of variations (e.g., ratio of the standard deviation to the mean) presented in Table 1.

Table 1. Mean and coefficient of variation of geyser heights

Vertical pipe length (m)	Average geyser height (m)	Coefficient of varience (%)
3	4.3	34.9
6	12.3	27.6
9	23.0	12.6
12	24.9	14.1

The data collected in the experiments included water temperature, air temperature, pressure heads at various locations inside the horizontal and vertical pipe, and the maximum geyser height, which is measured from the top of the vertical pipe. The maximum geyser height is determined from the video recordings using a known reference length located in the vertical pipe (i.e., distance from top of vertical pipe to pressure transducer located 0.76 m below it). The eruption height was calculated using the MATLAB image processing toolbox by utilizing the pixel dimension of the reference length. The geyser velocity at the top of the vertical pipe was not directly measured in the experiments.

©2019, IAHR. Used with permission / ISSN 2521-7119 (Print) - ISSN 2521-716X (Online) - ISSN 2521-7127 (USB)

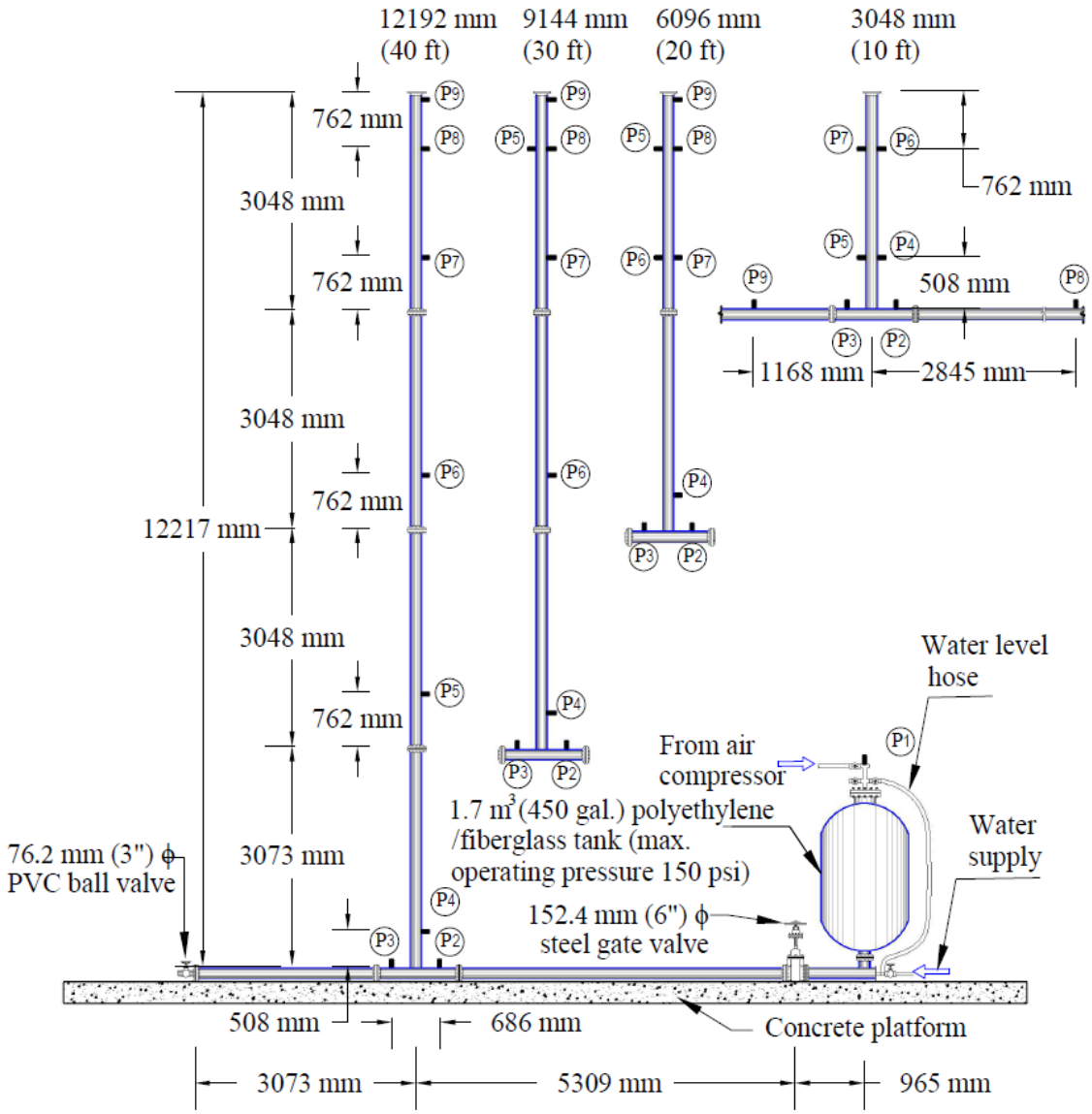

Figure 1. Sketch of experimental setup (Not To Scale), where P1 indicates the location of pressure transducer 1 and so on.

2.2 Experimental procedure

The experimental procedure was as follows:

i. Keeping the gate valve fully closed, the upstream tank is partially filled with water.
ii. The upstream tank is pressurized with air to a pre-specified pressure and the data acquisition system (DAQ) started to acquire data. The pre-specified pressure was obtained by iteration in such a way that (1) the steel gate valve can be fully opened slowly (~ 20-50 seconds) without releasing air from the tank, and (2) after the gate valve is fully opened, the water level in the tank is at its bottom (i.e., air has occupied the entire tank). The latter condition is necessary to produce a geyser. If after opening the valve, the water level in the tank was significantly above its bottom, geysering did not occur as the air in the tank was never admitted into the horizontal pipe.
iii. Once the gate valve is fully opened and the water level is at the bottom of the tank, the system is in apparent equilibrium. This is the case for both initial water volumes and hence, no distinction is made between both water volumes. Shortly after the aforementioned apparent equilibrium, the air-water interface at the bottom of the air tank oscillates up and down slightly which quickly grows and then leads to the air admission from the air tank to the horizontal pipe. The geyser eruptions would occur shortly after the air admission, which would occur between ten seconds to one minute after the gate valve is fully opened. Figure 2 shows an example of the complete time trace of pressure heads recorded for a vertical pipe length of 6 m. In this figure, the horizontal pipe downstream of the gate and the dropshaft are initially dry. At about 17 seconds, the gate opening is started and the gate is completely opened at about 60 seconds. As can be seen in Fig. 2, the sensors downstream of the gate and those in the dropshaft started to get submerged with water at a time between 29 and 38

©2019, IAHR. Used with permission / ISSN 2521-7119 (Print) - ISSN 2521-716X (Online) - ISSN 2521-7127 (USB)

seconds. Between 40 and 52 seconds there was significant water spill on top of the dropshaft. At about 55 seconds, the water spill at the top of the dropshaft ceased almost completely. At this time (55 s), the water level in the tank was at its bottom and air has not entered yet to the horizontal pipe. Between 60 and 74 seconds, the system is in apparent equilibrium as observed by the constant pressure heads in the tank (transducer P1) and the horizontal pipe (transducers P2 and P3), which pressure heads are equal to the vertical pipe length. During the first few seconds of this time interval (60-74 s), the air-water interface at the bottom of the air tank oscillates up and down slightly which quickly grows and then leads to the air admission from the air tank to the horizontal pipe. At about 70 seconds, the air in the tank started to be admitted continuously into the horizontal pipe and the geyser eruptions occurred between 76.5 and 82 seconds.

iv. After the eruptions, the system is depressurized and the data recording is stopped.

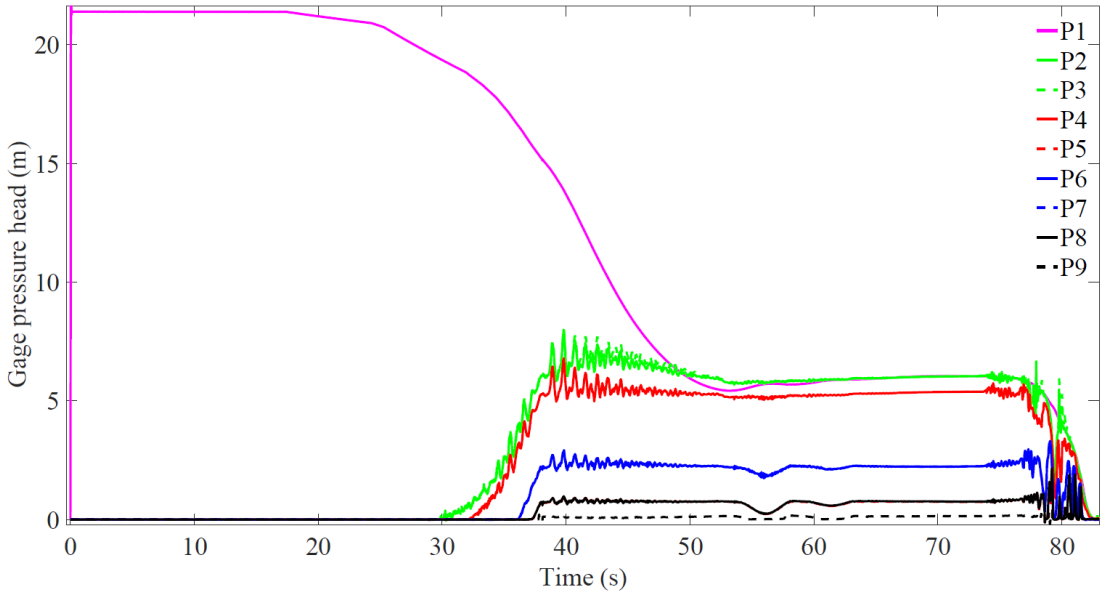

Figure 2. Example of complete time trace of pressure heads recorded for a vertical pipe length of 6 m.

2.3 Mechanisms leading to geysers

This section briefly describes the mechanisms leading to geysers as observed in the experiments. For an in-depth analysis of the geyser mechanisms including a mathematical model for estimating the maximum velocity of geyser eruption, the reader is referred to Leon (2018). The schematics for our theory on geyser mechanisms is presented in Figure 3, which summarizes the geyser processes in six parts (Figure 3a-3f.) For supplementing the theory, video snapshots for the horizontal pipe are presented in Figure 4. For supplementing the explanation, pressure head data is shown in Figure 5. The video snapshots in Figure 4 correspond to the pressure heads shown in Figure 5. For maximizing the view of the pressure heads, Figure 5 does not show the complete time trace of the experiment, however this figure shows part of the steady state period right before the air in the tank starts to be admitted into the horizontal pipe to produce the geyser. The main mechanisms that lead to geysering are summarized next:

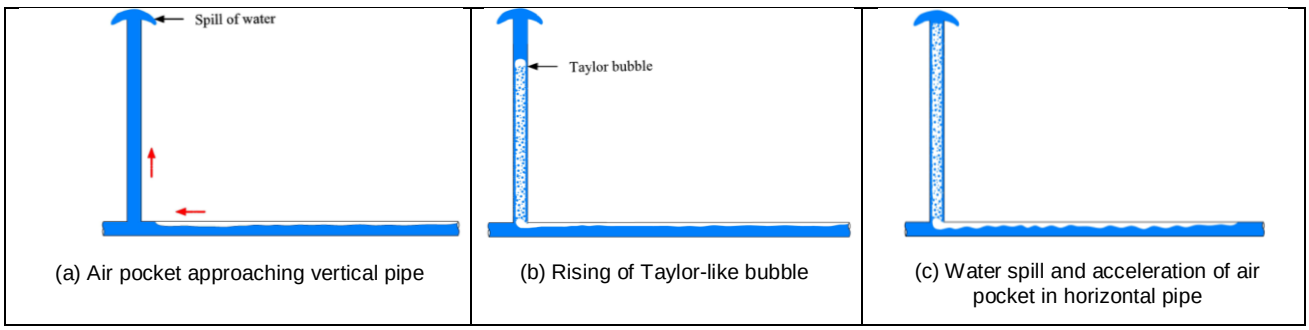

(a) Air pocket approaching vertical pipe

(b) Rising of Taylor-like bubble

(c) Water spill and acceleration of air pocket in horizontal pipe

©2019, IAHR. Used with permission / ISSN 2521-7119 (Print) - ISSN 2521-716X (Online) - ISSN 2521-7127 (USB)

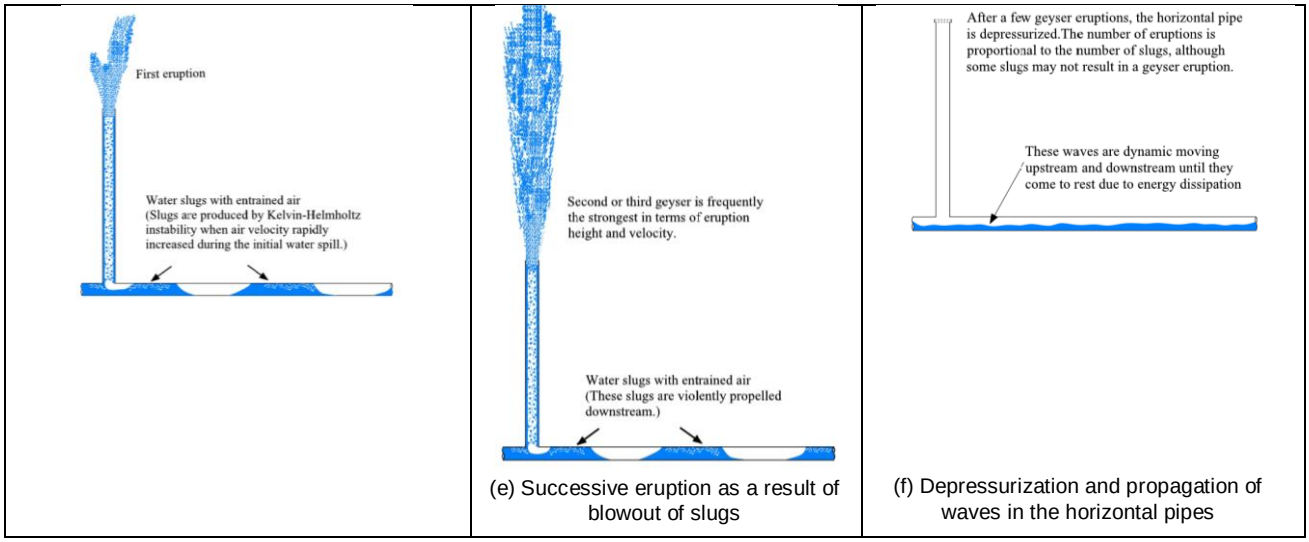

(e) Successive eruption as a result of blowout of slugs

(f) Depressurization and propagation of waves in the horizontal pipes

Figure 3. Schematic summarizing the geyser processes

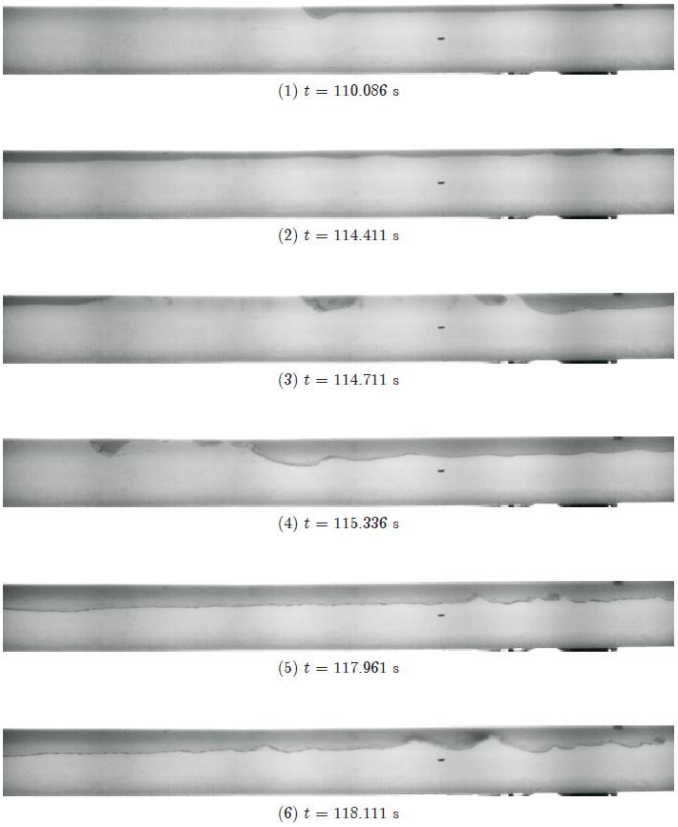

Figure 4. Flow snapshots in the horizontal pipe at various times

i. A large air pocket approaches the vertical pipe causing a small water spill at the top of the vertical pipe (Figure 3a and 4.1 [t = 110.086 s]). The movement of the air pocket in the horizontal pipe is relatively slow because there is no initial significant pressure gradient between the horizontal and vertical pipe.

ii. The large air pocket enters the vertical pipe and rises due to buoyancy causing more water spill at the top of the vertical pipe. The front of the air pocket, which resembles the classical Taylor bubble, occupies almost the entire cross-sectional area of the vertical pipe. The tail of the air pocket ascending in the vertical pipe is highly turbulent with a near homogenous mixture of air and water with great content of void fraction. In a similar way to the classical Taylor bubble, as the air pocket ascends, a significant amount of liquid that is on top of the air pocket is carried upwards and a portion of the water falls on the sides of the pocket (e.g., film flow).

©2019, IAHR. Used with permission / ISSN 2521-7119 (Print) - ISSN 2521-716X (Online) - ISSN 2521-7127 (USB)

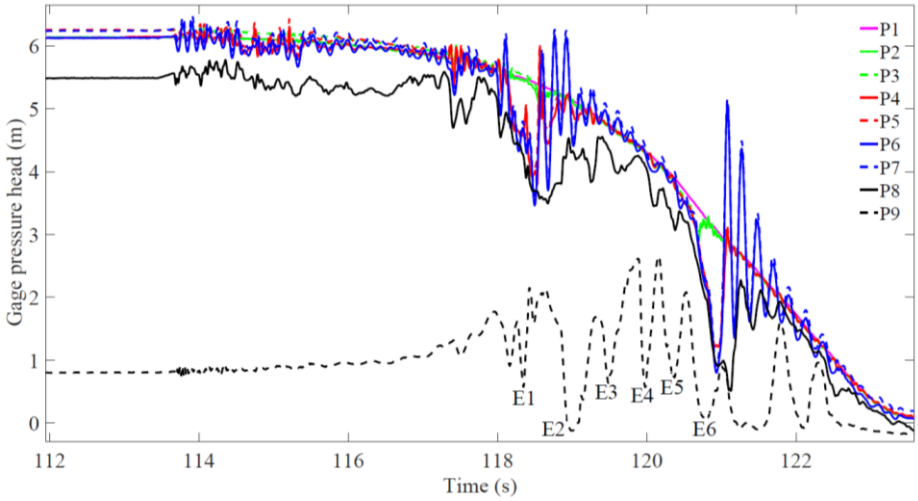

Figure 5. Example of detail of pressure heads during a geyser experiment (vertical pipe length = 6 m).

iii. When the Taylor-like bubble reaches the top of the vertical pipe, most of the water that is on top of the air pocket is spilled (Figure 3c).

iv. As water is quickly lost due to spilling, the hydrostatic pressure in the vertical pipe is rapidly reduced, creating a significant pressure gradient between the horizontal and vertical pipe, which accelerates the air in the horizontal pipe. This rapid acceleration propagates to the vertical pipe and leads to an eruption of a height which is not the largest (Figure 3d). Subsequently, the rapid increase in air velocity in the horizontal pipe results in the Kelvin-Helmholtz instability that transforms the initial stratified flow regime to wavy and eventually, slug flow. A slug flow is a series of liquid plugs (slugs with some entrained air) separated by relatively large air pockets (Elperin & Fominykh, 1996). It is worth mentioning that even though the vertical pipe is initially filled with water, the geyser will not be produced until part of the water in the vertical pipe is spilled. The geyser eruptions are distinguished as E1, E2, E3 and so on in Figure 5. These eruptions are evidenced by a sudden depressurization of pressure transducer P9, which is located near the top of the vertical pipe.

v. Once the slugs are formed in the horizontal pipe, there is a flow discontinuity and the continuous supply of air from the horizontal to the vertical pipe is blocked. Starting with the slug closest to the vertical pipe, in consecutive order and one at a time, the slugs are violently propelled into the vertical pipe right after each sudden drop of pressure in the vertical pipe (e.g., after a significant pressure gradient between the slug and the vertical pipe). It is worth mentioning that the liquid slugs supply the water for the eruptions. Overall, the second or third geyser has the largest intensity in terms of height (Figure 3e).

vi. After the second or third eruption, there may be a few more eruptions. However, as water is depleted in the vertical pipe and the horizontal pipe is depressurized, the geysering process is terminated. On average, between 3 to 8 eruptions in a time frame of 2 to 10 seconds has been observed.

3 NUMERICAL MODEL

The current study utilizes OpenFOAM (CFD Direct, 2017) to numerically investigate geysers presented in Leon et al. (2018). OpenFOAM offers a set of C++ libraries for solving partial differential equations and provides several solvers for CFD applications. A compressible two-phase flow solver called compressibleInterFoam (CIF) was used in this study to simulate geysers. CIF is suitable for modeling two compressible and immiscible fluids (CFD Direct, 2017). CIF employs an interface capturing approach using a Volume Of Fluid method for simulating interactions between two fluids. In the present paper, these two phases are water and air which are denoted by *w* and *a* subscripts, respectively. The properties of fluids are calculated for the mixture of two fluids based on the volume fraction of each phase. The conservation laws of mass, Eq. [1], momentum, Eq. [2] and energy, Eq. [3], for a homogeneous mixture are implemented in OpenFOAM as follows (Ma et al. 2016):

$$\frac{\partial \rho}{\partial t} + \nabla \cdot (\rho \boldsymbol{U}) = 0 \quad [1]$$

$$\frac{\partial \rho \boldsymbol{U}}{\partial t} + \nabla \cdot (\rho \boldsymbol{U}\boldsymbol{U}) - \nabla \cdot (\mu \nabla \boldsymbol{U}) = \sigma k \nabla \alpha - \boldsymbol{g} \cdot \boldsymbol{x} \nabla \rho - \nabla p_d \quad [2]$$

$$\frac{\partial \rho T}{\partial t} + \nabla \cdot (\rho \boldsymbol{U} T) - \nabla \cdot (\alpha_t \nabla T) = -\left(\frac{\alpha}{C_{v,a}} + \frac{1-\alpha}{C_{v,w}}\right)\left(\frac{\partial \rho k}{\partial t} + \nabla \cdot (\rho \boldsymbol{U} k) + \nabla \cdot (\boldsymbol{U} p)\right) \quad [3]$$

©2019, IAHR. Used with permission / ISSN 2521-7119 (Print) - ISSN 2521-716X (Online) - ISSN 2521-7127 (USB)

where $\boldsymbol{U}$ is the velocity vector, k is the curvature of the interface, $\boldsymbol{g}$ is the gravitational acceleration vector, $\boldsymbol{x}$ represents the position vector; p_d is the dynamic pressure, $c_{v,w}$ and $c_{v,a}$ are specific heat capacities of water and air, respectively; α_t is thermal eddy diffusivity, σ is the surface tension and K represents the specific kinetic energy. For the turbulence closure, the k-ε model is implemented in OpenFOAM based on Shih et al. (1995). Chegini et al. (2018) showed that this is the most suitable model for simulating geyser events in vertical shafts. Moreover, the discretization of the governing equations in OpenFOAM is based on a finite volume approach on collocated grid layout, i.e. all variables are located on the same grid point (Meier et al., 1999). Solution algorithm of CIF is based on a predictor-corrector method called pressure implicit split operator (PISO) (Issa, 1986). The PISO algorithm allows full coupling of velocity and pressure in each time-step which is necessary for transient simulations. In the current study, a second order scheme with a flux limiter (Van Leer, 1997) was considered for the spatial discretization and a second-order scheme for the temporal discretization called Crank-Nicolson. Additionally, the maximum Courant number was set to 0.5 (Chegini and Leon 2019).

A 3D mesh of the geometry of the experimental setup in Leon et al. (2018) was generated using SALOME (Open Cascade, 2017) and snappyHexMesh, an OpenFOAM meshing utility. The mesh is structured, as it is generally more suitable for multiphase flow simulations (Bayon et al., 2016), and hexahedral dominant. Regarding boundary conditions, the no-slip boundary condition is applied on the walls for the velocity field and zero gradient for the other fields. On the atmospheric domain, the total pressure (sum of static and dynamic pressures) is set to a fixed value of 102,032Pa (the atmospheric pressure reported in Leon et al. 2018) and other fields are set to zero gradient. The validation and subsequent numerical investigations were performed based on three criteria: spatial dimensions (2D and 3D), initial pressure head difference and compressibility of phases. A mesh convergence study was carried out to determine the most efficient mesh size in terms of accuracy and computation time. For the 2D simulations, a 2D mesh of the geometry was generated using the blockMesh utility of OpenFOAM. It is noted that four different vertical shaft lengths, were used in the laboratory experiments, one of which (6 m) was selected for the numerical study. The configuration used in the numerical simulations are denoted by a two-letter abbreviation, e.g. SD=2D and PD=0.05 means that the simulation is performed in 2D and the initial pressure head difference is 0.05 m. The validity of the numerical model for simulating geyser events was verified using the experimental data in Leon et al. (2018). The data used for the validation included geyser height and pressure head data of two pressure transducers P1 on the top of the air tank and P4 at the bottom of the vertical shaft. The average laboratory geyser height for the 6 m vertical shaft was 12.25 m and the error was ± 0.87 m.

4 CONSIDERATIONS FOR NUMERICALLY EFFICIENT MODELING OF GEYSERS

4.1 Spatial Dimensions

Even though geyser flows are thought to be highly three-dimensional, to investigate whether geysers could be represented with good accuracy in 2D, two simulations were carried out in 2D and 3D under similar numerical conditions and compared with the experiments in Leon et al. (2018). A quantitative comparison between 2D and 3 D models for one of the experiments is provided in Fig. 6 and Table 2. A qualitative comparison of 2D and 3D numerical results shows that the 2D model captures reasonably well the flow pattern transitions that occur during the formation of geysers. Moreover, the comparison of pressure traces and geyser height shows that both 2D and 3D simulations are in good agreement with the experimental data. This is an exciting and promising finding since the length scales of stormsewer systems is typically in the order of thousands of meters so the use of a 3D model for simulating geyser events is computationally very expensive and not practical. A 2D model, if established to be accurate for simulating geysers, could be an effective and a practical tool, especially for qualitative studies. It is clear that actual stormsewer systems are more complex than the experimental setup in Leon et al. (2018) in terms of geometry and boundary conditions and thus, further studies are needed before the 2D model is recommended for simulating geysering events.

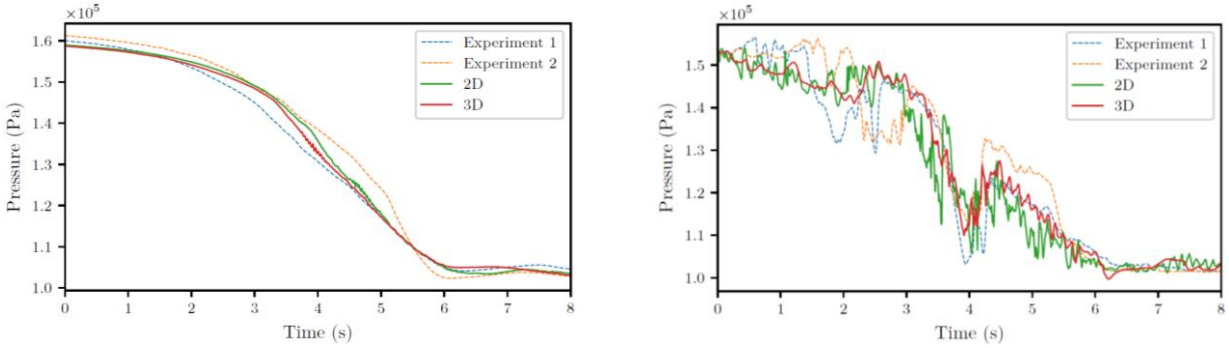

©2019, IAHR. Used with permission / ISSN 2521-7119 (Print) - ISSN 2521-716X (Online) - ISSN 2521-7127 (USB)

Figure 6. Numerical (2D and 3D) and experimental pressure results at two locations (PD=0.05, CW=compressible)

Table 2. Comparison of 2D and 3D simulations

Sample	U_{max} (m/s)	h_g (m)	E (%)	t_p (s)	t_s (min)
2D	32.62	11.31	7.7	25.83	63
3D	34.12	11.62	5.1	22.30	4725

PD=0.05, CW=compressible

4.2 Initial pressure head difference

In the experimental tests in Leon et al. (2018), right before air entered the horizontal pipe, the water and air were quiescent and in an apparent equilibrium. According to the pressure head traces in Leon et al. (2018), right before the air entered the horizontal pipe, the pressure difference between the air tank (P1) and the bottom of the vertical shaft (P4) was almost zero for all the experimental runs. In the numerical simulations, a "small" pressure head difference is required to push the air into the horizontal pipe. In order to determine this "small' required initial pressure head difference for accurate simulation of the experiments, a sensitivity analysis was performed. The results show that the geyser characteristics are similar when the initial pressure head difference is below 0.1 m (1.6% pressure head slope). However, for larger initial pressure head differences, the pressure traces and geyser height predictions deviate significantly from the experiments. Moreover, an initial pressure head difference of 0.1 m, speed up the simulation by about 30% compared to a pressure head difference of 0.01 m. It is noted that this threshold is obtained for the specified geometry and boundary conditions, and might be different for other conditions. Moreover, considering that the results with a 0.05 m initial pressure head difference are in better agreement with the experimental data compared to the 0.1 m case and given that the computation time difference between these two cases is not substantial, the 0.05 m initial pressure difference (0.8% initial pressure head slope) is deemed as the efficient value.

4.3 Compressibility

Generally, for single phase flows compressibility could be neglected in numerical simulations based on Mach number while in multiphase flows such assumption should be investigated. In the case of geysering, the dynamics of air pockets in the horizontal pipe and the vertical shaft plays a key role in the formation of geysers (Leon, 2018). Moreover, rapid changes in pressure and velocity fields during the geysering may lead to sudden and significant expansions and contractions of the air phase. To study the importance of compressibility of the phases in geysering four scenarios were considered; both phases as incompressible/compressible and only one phase as incompressible. The obtained results indicate that when both phases were considered incompressible, the model was unable to produce a geyser. The same holds true for the case where only air was considered incompressible. By setting only water as incompressible, however, the model successfully produced geysers which demonstrates the importance of compressibility of air. Obviously, the case where both phases were compressible was also able to simulate geysering. Figure 7 and Table 3 compares the results of these two successful cases with the experimental data. As observed, both successful cases [(1) water and air are compressible, (2) air is compressible and water is incompressible] are in good agreement with the experimental data, although the incompressible water case presents slightly stronger fluctuations. This is not surprising as very rapid flow changes (e.g., geyser flows) are not well represented by models that neglect water compressibility and those models are often overly conservative of pressure changes (Jung and Karney 2016). Considering that the computational effort for both successful cases are almost the same while the case where air and water are considered compressible is more accurate, this case was deemed as the most efficient option.

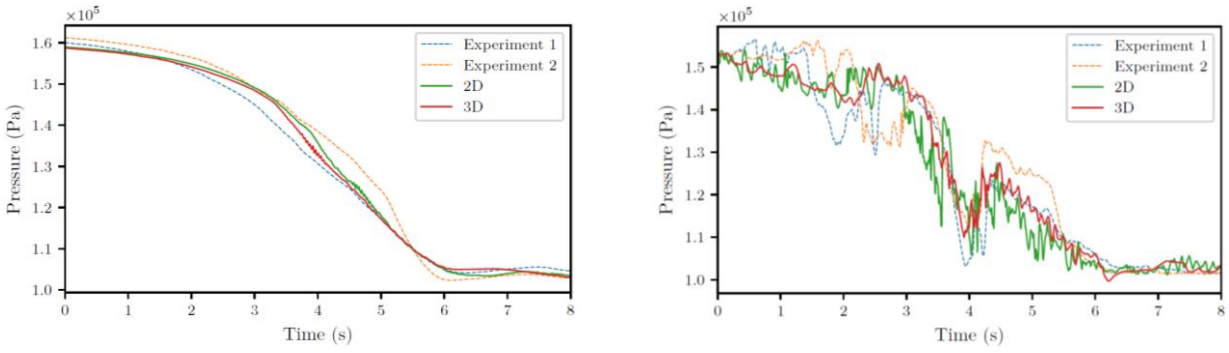

Figure 7. Results of simulations with water phase being considered incompressible and compressible at pressure probes (a) P1 and (b) P4 (SD=2D, PD=0.05)

©2019, IAHR. Used with permission / ISSN 2521-7119 (Print) - ISSN 2521-716X (Online) - ISSN 2521-7127 (USB)

Table 3. Comparison of simulations with water phase being considered incompressible and compressible

CW	U_{max} (m/s)	h_g (m)	E (%)	t_p (s)	t_s (min)
Compressible	32.62	11.31	7.7	25.83	63
Incompressible	33.11	11.46	6.4	24.61	62

SD=2D, PD=0.05

5 CONCLUSIONS

This paper reports a laboratory and numerical study on violent geysers in a vertical pipe. The laboratory work has produced violent geysers with characteristics resembling those geysers that occur in actual stormwater and combined sewer systems. The numerical study has investigated the characteristics of geysers using OpenFOAM. The model was validated using experimental data in Leon et al. (2018). The key results are as follows:

i. Geysers are driven not only by the flow dynamics in the vertical shaft but also in the horizontal pipe. Once the air pocket breaks through the free surface and produces a water spill, the horizontal pipe flow dynamics, in particular the rapidly changing pressure gradient following the first weak eruption, drives the geyser eruptions.
ii. Although geysering is often considered an intrinsically 3D phenomenon, the geyser experiments in Leon et al. (2018) was modeled in 2D with good accuracy. Further work is needed to verify the applicability of 2D models for simulating geysers in actual stormsewer systems.
iii. Air compressibility is crucial for simulating geysers events, while water compressibility is not.

ACKNOWLEDGEMENTS

This work was supported by the U.S. Environmental Protection Agency [grant R835187].

REFERENCES

Bayon, A., Valero, D., Garcia-Bartual, R., Valles-Moran, F.J., and Lopez-Jimenez, P.A. (2016). Performance assessment of OpenFOAM and FLOW-3d in the numerical modeling of a low Reynolds number hydraulic jump. *Environmental Modelling & Software*, 80:322–335.

CFD Direct (2017). OpenFOAM 5.0. The OpenFOAM Foundation Ltd, London, United Kingdom.

Chan, S.N., Cong, J., and Lee, J.H.W. (2018). 3D numerical modeling of geyser formation by release of entrapped air from horizontal pipe into vertical shaft. *Journal of Hydraulic Engineering*, 144(3):04017071.

Chegini, T. and Leon, A.S. (2019). Numerical Investigation of Field-Scale Geysers in a Vertical Shaft. *Journal of Hydraulic Research.* Accepted.

Chegini, T., Phan, M.K., and Leon, A.S. (2018). "Comparison of Various Turbulence Models for Violent Geysers in Vertical Pipes." In proceedings of *2018 ASCE-EWRI World Environmental & Water Resource Congress*, 99-108, Minneapolis, MN, June 3-7, 2018.

Choi, Y.J., Leon, A.S., and Apte, S.V. (2014). Three-dimensional numerical modeling of air-water geyser flows. In World Environmental and Water Resources Congress 2014. *American Society of Civil Engineers*.

Cong, J., Chan, S.N., and Lee, J.H.W. (2017). Geyser formation by release of entrapped air from horizontal pipe into vertical shaft. *Journal of Hydraulic Engineering*, 143(9):04017039.

Elperin, T., & Fominykh, A. (1996). Effect of gas release and condensation on characteristics of two-phase gas and vapor-liquid slug flow. *Heat and Mass Transfer*, 31 (6), 387-391.

Guo, Q., & Song, C.S.S. (1991). Hydrodynamics under transient conditions. *J. Hydraul. Eng*, 117 (8), 1042-1055.

Hamam, M.A., & McCorquodale, J.A. (1982). Transient conditions in the transition from gravity to surcharged sewer flow. *Can. J. Civ. Eng*., 9, 189-196.

Issa, R. (1986). Solution of the implicitly discretised fluid flow equations by operator-splitting. *Journal of Computational Physics*, 62(1):40–65.

Jung, B.S. and Karney, B. (2016). A practical overview of unsteady pipe flow modeling: from physics to numerical solutions. *Urban Water Journal*, 14(5):502–508.

Leon, A.S. (2016). Mathematical models for quantifying eruption velocity in degassing pipes based on exsolution of a single gas and simultaneous exsolution of multiple gases. *J. volcanology and geothermal research*, 323 (1), 72-79.

Leon, A.S. (2018). Mechanisms that lead to violent geysers in vertical shafts. *Journal of Hydraulic Research*. Accepted.

Leon, A.S. (2018), Elayeb I. S., Tang, Y. (2018). An experimental study on violent geysers in vertical pipes. *Journal of Hydraulic Research*. Accepted.

©2019, IAHR. Used with permission / ISSN 2521-7119 (Print) - ISSN 2521-716X (Online) - ISSN 2521-7127 (USB)

Lewis, J.M. (2011). A physical investigation of air/water interactions leading to geyser events in rapid filling pipelines (Unpublished doctoral dissertation). University of Michigan.

Ma, Z., Causon, D., Qian, L., Mingham, C., and Ferrer, P.M. (2016). Numerical investigation of air enclosed wave impacts in a depressurised tank. *Ocean Engineering*, 123:15–27.

Meier, H., Alves, J., and Mori, M. (1999). Comparison between staggered and collocated grids in the finite-volume method performance for single and multi-phase flows. *Computers & Chemical Engineering*, 23(3):247–262.

Open Cascade (2017). SALOME 8.2. Open Cascade Inc., Guyancourt, France.

Shao, Z.S. (2013). Two-dimensional hydrodynamic modeling of two-phase flow for understanding geyser phenomena in urban stormwater system (Unpublished doctoral dissertation). University of Kentucky, Lexington, KY.

Shih, T.H., Liou, W.W., Shabbir, A., Yang, Z., and Zhu, J. (1995). A new k-ε eddy viscosity model for high reynolds number turbulent flows. *Computers & Fluids*, 24(3):227–238.

Van Leer, B. (1997). Towards the ultimate conservative difference scheme. *J. Comput. Phys.*, 135(2):229–248.

Vasconcelos, J.G. (2005). Dynamic approach to the description of flow regime transition in stormwater systems (Unpublished doctoral dissertation). University of Michigan.

©2019, IAHR. Used with permission / ISSN 2521-7119 (Print) - ISSN 2521-716X (Online) - ISSN 2521-7127 (USB)